Measurement of the Ocean Wave–Radar Modulation Transfer Function at 35 GHz From a Sea-Based Platform in the North Sea

F. Feindt

Institut für Meereskunde, Universität Hamburg, Federal Republic of Germany

J. Schröter

Max-Planck-Institut für Meteorologie, Hamburg, Federal Republic of Germany

W. Alpers

Fachbereich 1 (Physik), Physik des Meeres, Universität Bremen, Federal Republic of Germany

The ocean wave–radar modulation transfer function (MTF) at 35 GHz (K_a band) was measured with a coherent pulsed Doppler scatterometer from a research platform in the North Sea. The Bragg waves corresponding to this radar freqency at intermediate incidence angles are capillary waves with a wavelength of about 0.5 cm. During the experiment the air-sea temperature varied between $-1°C$ and $-5°C$, which implies that the boundary layer at the air-sea interface was unstable. The measurements at 35 GHz yield the following results: The modulus of the dimensionless MTF decreases with increasing wind speed and is larger for horizontal (HH) than for vertical (VV) polarization. The value of the dimensionless MTF for HH polarization varies between 3.5 and 9.5 in the frequency range between 0.11 and 0.14 Hz, and that for VV polarization varies between 2.5 and 7.5 depending on wind speed. The phase of the MTF for HH polarization is such that the maximum of the radar return originates from the leeward (forward) face of the long ocean waves between 0° and 15° away from the wave crests. The phase of MTF for VV polarization lies between $-75°$ and $-30°$, which means that the maximum of the radar return originates from the windward (rear) face of the long ocean waves. We conclude that the phase dependence of the K_a band MTF implies that the maximum of the hydrodynamic modulation for these capillary waves occurs at the windward face of the long ocean waves. The nonuniform distribution of the 0.5-cm waves with respect to the long ocean wave profile is probably caused by a wave-induced spatially variable air flow.

1. Introduction

The ocean wave–radar modulation transfer function relates the variation of the radar cross section to the height or slope of the long ocean surface waves. This knowledge is required, for example, when converting radar image intensity spectra of ocean scenes into ocean wave height spectra. Radar imagery at X and L band of ocean surface wave fields has been generated extensively from airplanes (see, for example, e.g., *Elachi* [1978], *Schemdin et al.* [1978], and *Shuchman et al.* [1983]) and at L band also from spaceborne platforms (Seasat and space shuttle). This has led to the necessity to perform measurements of the ocean wave–radar modulation transfer function at these radar frequencies.

The first measurements of the water wave–radar MTF have been carried out in a wind-wave tank by *Keller and Wright* [1975] at the Naval Research Laboratory in Washington, D. C. Subsequently, such measurements have also been performed in the open ocean from sea-based platforms [*Plant et al.*, 1978; *Alpers and Jones*, 1978; *Wright et al.*, 1980; *Plant et al.*, 1983]. All these measurements have been made with scatterometers operating at frequencies of 9.375 GHz (X band) and 1.5 GHz (L band).

Here we report for the first time about measurements of the ocean wave–radar modulation transfer function at K_a band (35 GHz). Apart from the fact that it can serve to convert K_a band radar image intensity spectra into ocean wave height

spectra, it also provides further insight into the hydrodynamic modulation of the short waves by the long ocean waves. The Bragg waves corresponding to this radar frequency have, at intermediate incidence angles, wavelengths of about 0.5 cm and thus are capillary waves, whereas the Bragg waves corresponding to L band are gravity waves, and the Bragg waves corresponding to X band are gravity-capillary waves.

We expect that capillary waves respond more strongly to wave induced wind fluctuations than gravity waves. Thus the K_a band MTF should exhibit a qualitatively different behavior from the X and L band MTFs.

2. The Experiment

The experiment reported here was carried out between December 2 and December 14, 1981, at the Forschungsplattform Nordsee, which is a German research tower located at 54°42.0′N and 7°10.0′E in the North Sea, approximately 70 km west of the island of Sylt (Germany). The water depth at this site is 30 m.

The scatterometer was a 35-GHz pulsed Doppler radar built completely in a semiconductor module technique. The parameters of this instrument are summarized in Table 1. In this experiment we used a pulse repetition frequency (PRF) of 66 kHz and a pulse length of 30 ns. The video output signals of the modulus and phase of the backscattered microwave signals were integrated using a low-pass filter with a time constant of 0.1 s. The spillover from the transmit circuit was eliminated by range gating. The video output of the AM channel giving the backscattered power is very close to logarithmic over a dynamic range of 60 dB. A parabolic antenna

TABLE 1. Parameters of the K_a Band Pulsed Doppler Radar Employed in This Experiment

	Comments
Frequency, GHz	35
Frequency stability, Hz	± 10
Pulse repetition frequency, kHz	66
Pulse length, ns	30
Peak power, W	1.5
Noise level of the receiver, dB	6
Dynamic range of the receiver, dB	60
Linearity, dB	± 1.5
Polarization	VV and HH
Weight, kg	30
Antenna	
Type	parabolic
Diameter, cm	30
Two-way 3-dB beam width, deg	2.0
Height above mean sea surface, m	30.5 m
Incidence angle, deg	60
Range antenna-sea surface, m	61
Footprint size, m^2	3.77 * 1.88

with a diameter of 30 cm was used for transmission and reception. The two-way 3-dB beam width was 2.0°. The antenna together with the scatterometer was mounted on the rail of the research platform at a height of 30.5 m above mean sea level (Figure 1). The incidence angle was kept fixed at 60°, resulting in an elliptical footprint with axis diameters of 3.77 m and 1.88 m.

The backscattered power originating from this footprint was measured together with the Doppler shift. The modulus and phase of the radar return was recorded on an analogue tape recorder for later processing.

The ocean wave–radar MTF has been obtained then by correlating the amplitude modulated (AM) part of the signal with its frequency modulated (FM) part. This is possible because the Doppler shift of the backscattered signal can be used for measuring the ocean wave height [see *Plant et al.*, 1978].

For comparison we also measured the nondirectional ocean wave spectrum with a resistive wave staff supported by a crane

on the northwest corner of the platform. The horizontal distance between this wave staff and the footprint of the antenna varied between 20 m (antenna pointing towards 270°N) and 30 m (antenna pointing towards 180°N).

During the experiment the wind speed and direction varied between 6.5 m/s and 18 m/s, and the wind direction between 300°N and 180°N. The wind was measured at the platform at a height of 46 m by a cup anemometer. The antenna was directed most of the time into the wind (upwind) and only in a few cases into the crosswind direction or intermediate wind directions.

During the whole experiment the water temperature was higher than the air temperature, so that the boundary layer at the air-sea interface was always unstable. The air-sea temperature difference varied between $-1°C$ and $-5°C$.

3. DEFINITION OF THE OCEAN WAVE–RADAR MODULATION TRANSFER FUNCTION

We assume that the power of the backscattered radar signal depends linearly on the long surface wave field. Then the radar cross section modulation can be described by a modulation transfer function $R(\mathbf{k})$. If we write the surface elevation associated with the long ocean waves and the radar cross section per unit area (normalized radar cross section, or NRCS) as Fourier integrals:

$$\zeta = \int [z(\mathbf{k})e^{i(\mathbf{k} \cdot \mathbf{x} - \omega t)} + \text{c.c.}] \, d\mathbf{k} \qquad (1)$$

$$\sigma = \sigma_0 + \int [\sigma(\mathbf{k})e^{i(\mathbf{k} \cdot \mathbf{x} - \omega t)} + \text{c.c.}] \, d\mathbf{k} \qquad (2)$$

then the complex modulation transfer function $R(\mathbf{k})$ is defined by:

$$\frac{\sigma(\mathbf{k})}{\sigma_0} = R(\mathbf{k}) \cdot z(\mathbf{k}) \qquad (3)$$

Here $\mathbf{k}$ denotes the wave vector, ω denotes the radian frequency of the long ocean wave field, and σ_0 denotes the average NRCS; c.c. stands for complex conjugation.
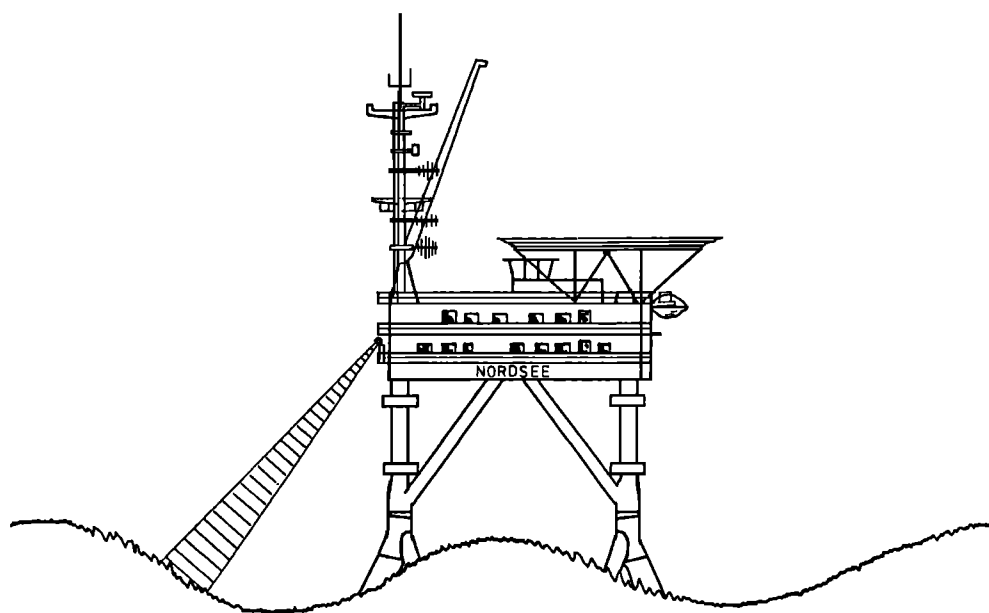

Fig. 1. Configuration of the experiment at the Forschungsplattform Nordsee (German Research Platform North Sea). The antenna of the K_a band radar illuminates an ocean patch of dimension 3.9 m × 1.9 m.

Note that the definition (equation (3)) implies that the surface elevation $\zeta(x)$ associated with the long waves and the cross-section variation $\sigma(x) - \sigma_0$ are linearly related. This means that the radar backscattering at long ocean surface waves can be modeled as a single-input linear system [*Bendat and Piersol* 1966, p. 98], which is a rather strong assumption. If linearity holds, then $R(k)$ is given by (see equation (3.138) of *Bendat and Piersol* [1966])

$$R(\mathbf{k}) = \frac{1}{\sigma_0} \frac{G_{\sigma,\zeta}(\mathbf{k})}{G_\zeta(\mathbf{k})} \tag{4}$$

Here $G_{\sigma,\zeta}$ denotes the cross-spectrum of σ and ζ, and G_ζ denotes the autospectrum (power or variance spectrum) of ζ. For practical purposes it is often more convenient to introduce a nondimensional modulation transfer function $\mathbf{M}(\mathbf{k})$ which is defined by [see *Schröter et al.*, 1986]

$$R(\mathbf{k}) = \mathbf{k} \cdot \mathbf{M}(\mathbf{k}) \tag{5}$$

Apart from a phase factor, $\mathbf{M}(\mathbf{k})$ is the MTF which relates the wave slope to the radar cross section modulation. This MTF reflects more physics of the modulation, since the cross-section modulation is primarily determined by the wave slope [*Alpers et al.*, 1981]. Note that our definition of $\mathbf{M}$ implies that the phase of $\mathbf{M}$ is equal to the phase of R.

However, the modulation transfer function $\mathbf{M}(\mathbf{k})$, which is a two-component, complex vector in two-dimensional wave vector space, is not measured in our experiment. In the experiment reported in this paper we measure the NRCS at a fixed incidence and azimuth angle, and we measure the ocean wave height as a function of time. This implies that the resulting modulation transfer function M is a complex scalar function which depends only on one variable, the ocean wave frequency.

As was mentioned before, we do not measure the wave height $\zeta(t)$ directly but infer it from the Doppler shift $f_d(t)$ inherent in the backscattered radar signal. This technique, which was introduced by J. W. Wright and coworkers at the Naval Research Laboratory in Washington, D. C. [see *Plant et al.*, 1978, 1983], has the advantage that only one instrument is needed for measuring the time series $\sigma(t)$ and $f_d(t)$.

A further advantage is that no phase lag occurs between the two time series because of spatial separation, since they originate from the same ocean patch. The transfer function $S(k)$ relating the Doppler shift f_d of the backscattered radar signal to the wave height is well known from the dynamics of ocean surface waves and is calculated in the appendix. The actually measured modulation transfer function N between $\sigma(t)$ and $f_d(t)$ is then related to M by

$$kM(k) = S(k)N(k) \tag{6}$$

where S is given by (A5), (A7), and (A8). Here $k = |\mathbf{k}|$ denotes the wave number of the long ocean wave which is related to the ocean wave frequency ω by the dispersion relation for water waves [*Phillips*, 1977, p. 37].

Our definition of the dimensionless ocean wave–radar modulation transfer function M differs slightly from the one used by the Naval Research Laboratory group [*Wright et al.*, 1980; *Plant et al.* 1983]. They conventionally define the MTF in terms of the cross spectrum between the backscattered power P and the component u of the orbital velocity in the direction of the wave propagation. Their definition of the MTF is

$$m = \frac{C_{ph}}{P_0} \frac{G_{P,u}}{G_u} \tag{7}$$

where $G_{P,u}$ denotes the cross spectrum between P and u, G_u denotes the power spectrum of u, C_{ph} denotes the phase speed of the ocean wave, and P_0 denotes the average backscattered power.

As is shown in appendix B of *Schröter et al.* [1986], m and M are related by $m = M \tanh (kD)$. Here D denotes the water depth. For deep water waves the two MTFs are identical, since $\tanh (kD) = 1$ for $D \to \infty$.

4. SIGNAL PROCESSING

The time series used for calculating the MTF have a length of 33 min. The analogue-recorded time series of the wave staff and of the AM channel of the scatterometer were sampled with a frequency of 10 Hz for digital processing on the Cyber 173 computer. Both time series were low-pass filtered with a cutoff frequency of 1 Hz.

To obtain the Doppler shift f_d, the time series of the FM channel of the scatterometer was sampled with a frequency of 1 kHz and divided into segments of 0.128 s. For every segment a Fourier spectrum was calculated with a frequency resolution of 8 Hz and two degrees of freedom. Then a new time series $f_d(t)$ was created by taking the position of the peak of the Doppler spectrum as a function of time. Power spectra of $f_d(t)$, $\sigma(t)$, and $\zeta(t)$ were calculated with a frequency resolution of 0.03 Hz and 120 degrees of freedom. All three time series, the Doppler shift, the radar backscattering cross section and the wave staff time series, were cross correlated with each other.

Since the coherence between the radar cross section and the wave-height measured by the wave staff was always very low owing to the large distance between the antenna footprint and the wave staff, we used only the cross spectra between the time series of the Doppler shift and the radar cross section to calculate the MTF. In the present analysis, only those spectral values have been used for computing the MTF for which the coherence was larger than 0.55 in a frequency range between 0.1 and 0.35 Hz. For frequencies below 0.35 Hz the diameter of the illuminated ocean patch is much smaller than the wavelength of the ocean waves, so that the Doppler shift can be used for measuring the orbital velocity of the long ocean waves.

Since the time series of the backscattered microwave power is measured in a logarithmic scale (decibels), the modulus of the dimensionless modulation transfer function is given by (see equation (6))

$$|M| = \frac{1}{10 \log e} \frac{1}{|\mathbf{k}|} |S(\mathbf{k})| \, |\gamma_{f_d, 10 \log \sigma}| \left(\frac{G_{10 \log \sigma}}{G_{f_d}} \right)^{1/2} \tag{8}$$

where $|S(\mathbf{k})|$ is given by equation (A7) and $\gamma_{f_d, 10 \log \sigma}$ denotes the coherence function between f_d and $10 \log \sigma$, which is defined by

$$\gamma_{f_d, \log \sigma} = \frac{G_{f_d, 10 \log \sigma}}{[G_{f_d} G_{10 \log \sigma}]^{1/2}} \tag{9}$$

When calculating the MTF, we must know the ocean wave spectrum in look direction of the antenna. But only little directional information is contained in the Doppler shift, since the geometric factor occurring in $S(k)$ (the last factor in (A7)) does not vary strongly with azimuth angle ϕ for intermediate incidence angles θ_i. We therefore approximate the long ocean waves field by a unidirectional field. (For a more detailed discussion, see *Schröter et al.* [1986, Appendix A]). Normally, wave and wind direction are nearly the same. But for the cases where a swell was present, the angle between ocean wave
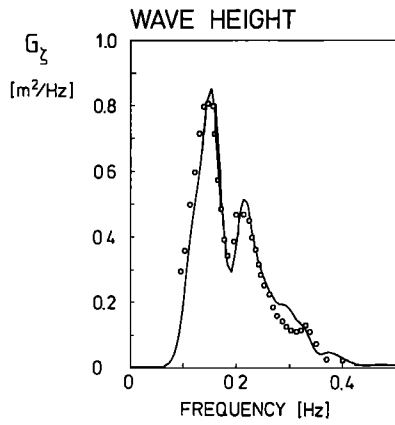
Fig. 2. Comparison of wave height spectra measured by wave staff (solid line) and by the scatterometer by means of the Doppler shift (circles).

propagation and antenna look direction was determined visually.

Figure 2 shows an example of an ocean wave spectrum measured both by a wave staff and by the Doppler shift of the backscattered microwave signal. In this particular case a swell and a wind sea were present. Equation (A11) was used to convert the Doppler spectrum into a wave height spectrum. Figure 2 clearly demonstrates that the FM channel of the scatterometer can be used for measuring ocean wave height spectra.

As was stated before, we use only those spectral values for calculating M for which the modulus of the coherence func-
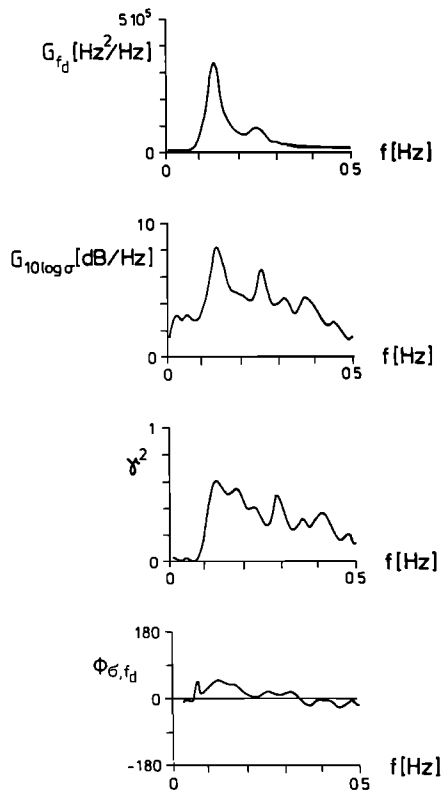
Fig. 3. Typical examples of measured power spectra of f_d, 10 log σ, of the square of the modulus of the coherence function γ^2, and the phase of cross spectrum of these two time series.
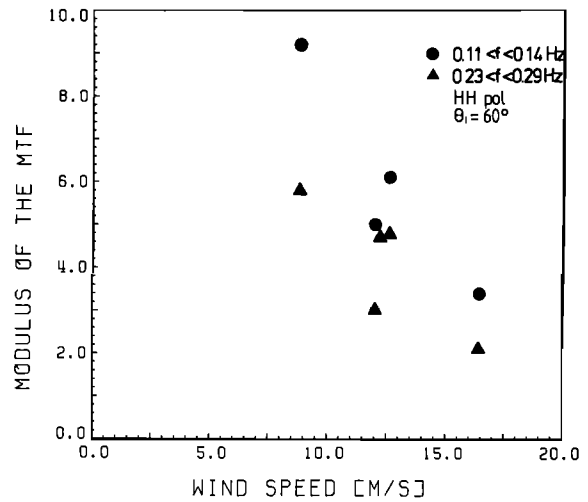
Fig. 4. Modulus of the dimensionless MTF as a function of wind speed for HH polarization and 60° incidence angle with the antenna pointing into the wind. The data points are divided into two frequency bins.

tion defined by (9), which we denote as γ, is larger than 0.55. With 120 degrees of freedom given, this means the modulus of the measured MTF lies between 0.50 and 1.66 times the true one (with 90% confidence limits, assuming the coherence function is true). A typical value for γ is 0.7, with corresponding 90% confidence limits of 0.65 and 1.4. Confidence intervals for the phase of M are $\pm 17°$ for $\gamma = 0.55$ and $\pm 11°$ for $\gamma = 0.7$.

5. RESULTS

Because of the weather situation encountered during the experiment, data could be collected only during moderate and high sea states.

In Figure 3, typical examples of measured power spectra of 10 log σ and f_d are shown together with the phase of the cross spectrum between 10 log σ and f_d and the square of the coherence function. The MTF is then calculated by using (8).

Figure 4 and Figure 5 show the wind speed dependence of the modulus of the MTF for HH and VV polarization, respectively. These measurements were taken at 60° incidence angle
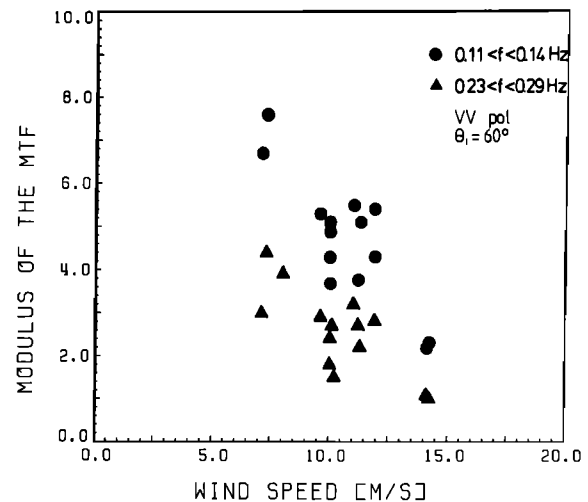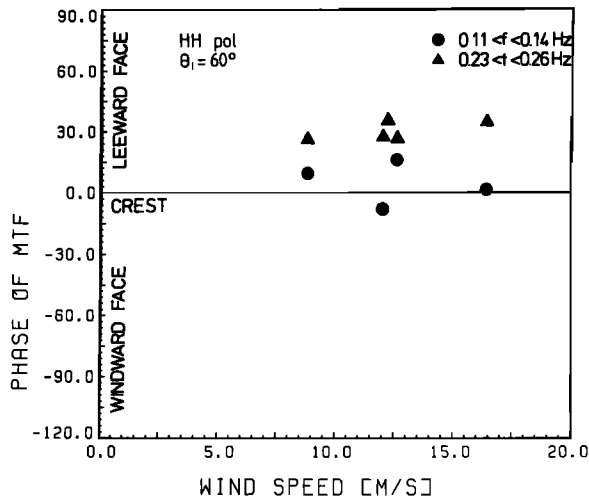

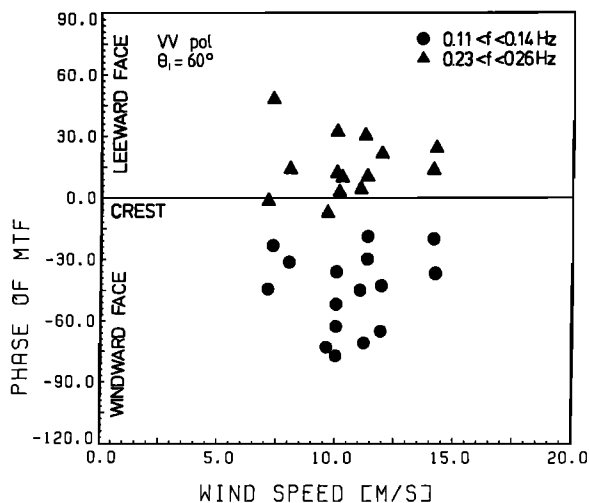Fig. 5. Same as Figure 4, but for VV polarization.

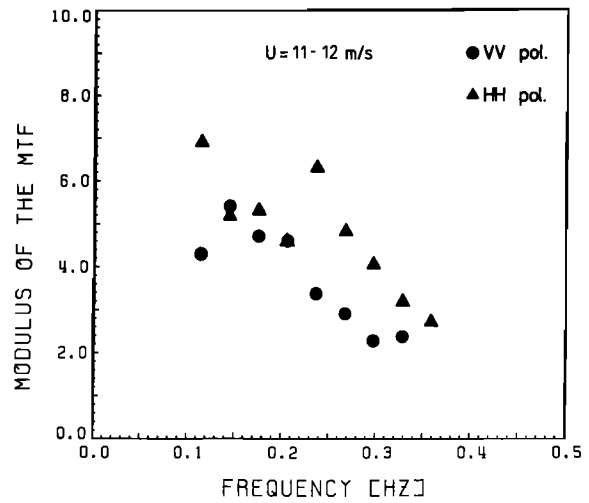Fig. 6. Phase of the dimensionless MTF of Figure 4.

Fig. 8. Modulus of the dimensionless MTF as a function of frequency for VV and HH polarization and 60° incidence angle with the antenna pointing into the wind. The wind speed is 11–12 m/s.

with the antenna pointing within ±30° into the wind direction. The data are separated into two ocean wave frequency bins of 0.11–0.14 Hz and 0.23–0.29 Hz. These figures show that the modulus of the dimensionless MTF decreases with increasing wind speed for both polarizations and that the modulus is larger for horizontal than for vertical polarization, as was predicted by theory [Alpers et al., 1981; Plant et al., 1983].

In Figure 6 the phase ϕ^M of the MTF for HH polarization is plotted as a function of wind speed. Though only few data are available, they seem to show that the phase ϕ^M is nearly constant as a function of wind speed. The maximum radar return at HH polarization in the frequency bin 0.11–0.14 Hz originates from the wave crest ($-5° < \phi^M < 15°$), and that in the frequency bin 0.23–0.26 Hz originates from the leeward face of the ocean wave, about 30° away from the crest.

The phase ϕ^M of the MTF for VV polarization with antenna looking upwind is plotted in Figure 7 as a function of wind speed. For frequencies between 0.11 and 0.14 Hz, the phase ϕ^M of the MTF is negative and varies between $-75°$ and $-15°$. This means that the maximum of the radar return

originates from the rear (windward or luffward) face of the long waves. For frequencies between 0.23 and 0.26 Hz the phase of the MTF is positive and varies between 0° and $+45°$. This means that the maximum of the radar return originates from the forward (leeward) face of the long waves. It seems that ϕ^M does not depend on wind speed.

For a wind speed of 11–12 m/s the frequency dependence of the modulus and phase of the MTF at both polarization is depicted in Figure 8 and Figure 9, respectively. Figure 8 shows that the modulus of the MTFs decrease with frequency. The corresponding phase plot (Figure 9) shows for example that at HH polarization and at $f = 0.1$ Hz the maximum radar return originates from the crest of the long wave. With increasing frequency the phase of the MTF is shifted towards the leeward face of the long waves.

For a wind speed of 16.4 m/s, the modulus of the MTF at HH polarization is shown in Figure 10. In this high wind speed case the frequency dependence of the modulus of the MTF is much smaller.

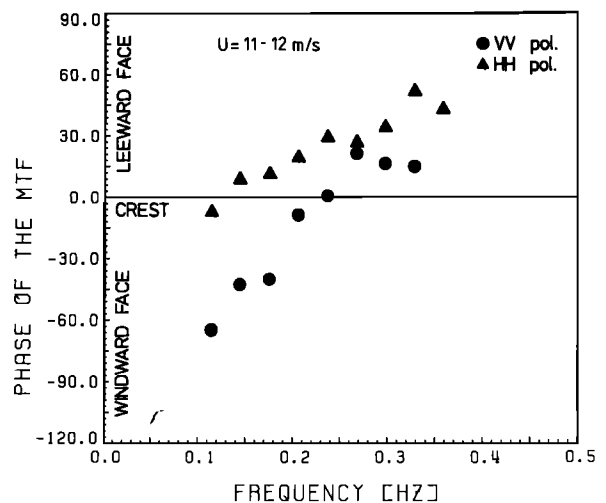Fig. 7. Phase of the dimensionless MTF of Figure 5.

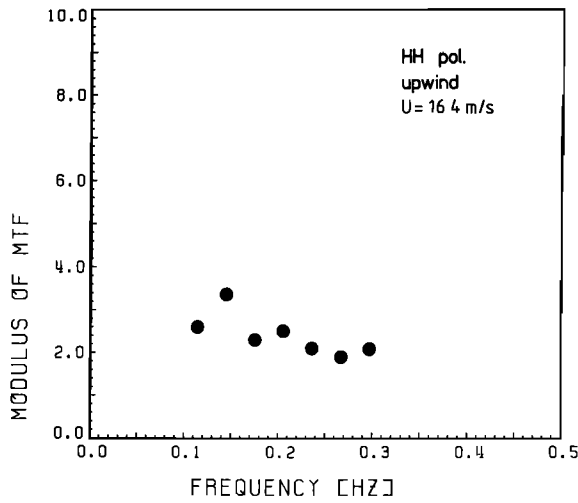Fig. 9. Phase of the dimensionless MTF of Figure 8.

Fig. 10. Modulus of the dimensionless MTF as a function of frequency for HH polarization and 60° incidence angle with the antenna pointing into the wind. The wind speed is 16.4 m/s.

Fig. 12. Comparison of the wind speed dependence of the phase of the MTFs at different microwave bands.

6. DISCUSSION

In Figure 11 and Figure 12 the dependence of the modulus and phase of the MTF at VV polarization on wind speed is shown for four different microwave frequencies. For this comparison we used L and X band (1.5 GHz and 9.3 GHz) data from *Plant et al.* [1983] and C band (4.3 GHz) data from *Schröter et al.* [1986]. These data are for incidence angles between 50° and 60° and for the antenna pointing into the wind direction. Figure 11 shows that for all four microwave frequencies the modulus of the MTF decreases with wind speed. Only small differences in the wind speed dependence of the MTF exist for the four microwave bands. However, this dependence seems to be weakest for L band. At high wind speeds the modulus of the MTF is larger for L and C band than for X and K_a band. Furthermore, the modulus of the MTF seems to decrease with increasing microwave frequency. Also, the phase of the K_a band MTF exhibits a slightly different behavior than the MTF phase in the other lower micro-
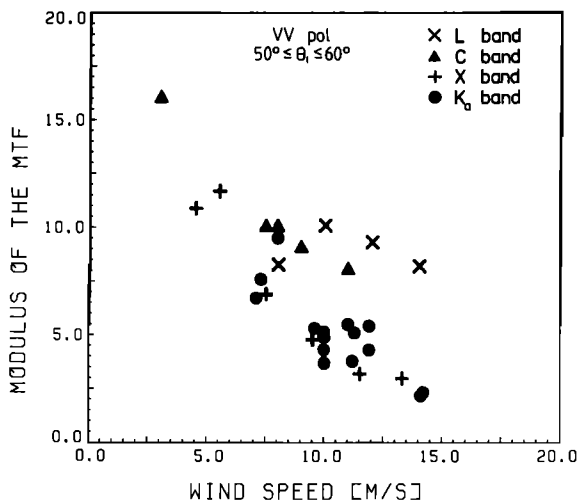

Fig. 11. Comparison of the wind speed dependence of the modulus of the dimensionless MTFs for different microwave bands (VV polarization, incidence angle between 50° and 60°, upwind conditions).
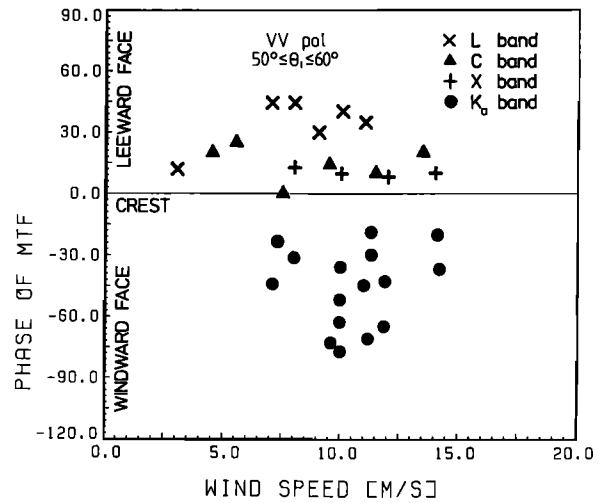
wave frequency bands. At X, C, and L band the strongest radar return originates from the leeward forward face near the crest of the long ocean waves ($0° < \phi^M < 45°$), and at K_a band the strongest return originates from the windward face of the long ocean wave ($-75° < \phi^M < -30°$) (see Figure 7).

In the two-scale wave model the MTF can be written as a sum of the tilt and the hydrodynamic MTF [*Keller and Wright*, 1975; *Alpers et al.*, 1981]

$$M = M_{\text{tilt}} + M_{\text{hydr}} \qquad (10)$$

The tilt MTF can be calcualted from Bragg scattering theory and is given for small slopes and for up-wave looking antenna by [see *Keller and Wright*, 1975; *Feindt*, 1985]

$$M_{\text{tilt}} = -i\left(\frac{1}{T}\frac{\partial T}{\partial \theta_i} + \frac{1}{\tan \theta_i}\frac{|\mathbf{k}|}{E}\frac{\partial E}{\partial |\mathbf{k}|}\right)\Bigg|_{\vec{n}=(0,0,1)} \qquad (11)$$

Here E denotes the spectral energy density of the Bragg waves; $\mathbf{k}$ denotes their wave number; $\vec{n}$ denotes the surface normal vector; and T denotes the Bragg scattering coefficient, which depends on the dielectric constant ε, the polarization, and the incidence angle θ_i. The first term in (11) is nearly the same for all four frequency bands considered here [see *Alpers et al.*, 1981]. However, the spectrum E in the capillary wave region is proportional to ω^{-2} [see *Kitaigorodskii*, 1970], whereas in the gravity wave region it is proportional to ω^{-5}.

Therefore the second term in (11) has a different value for K_a band than for L, C, or X band. For an incidence angle of 60° the theoretical value of the tilt modulation transfer function at VV polarization for K_a band is 0.5, while for L, C, and X band it is around 2. The range modulation gives a contribution which is less than 1 because of the large distance R between the antenna and the footprint ($R > 40$ m). Thus the theoretical range MTF and the tilt MTF at VV polarization are small in comparison with the measured modulation transfer function M.

Consequently, the main contribution to the MTF at VV polarization must originate from the hydrodynamic modulation of the Bragg waves by the long ocean waves. In particular, this applies for Bragg waves pertaining to K_a band scattering. The phase of the K_a band MTF is measured to lie between $-30°$ and $-75°$. This means that the maximum of the

amplitude modulation of the short waves is located on the rear or windward face of the long ocean waves. It is well known that capillary waves respond very fast to variations in wind speed. Therefore the K_a band Bragg wave should be affected more strongly by the wind than the X, C, and L band Bragg waves. It is thus conceivable that the nonuniform generation of short waves by a wave-induced spatially varying wind field may constitute a major contribution to the K_a band MTF. The capillary waves generated on the windward face of the long ocean waves can travel only a short distance, since they are dissipated very strongly by viscosity. The modulation of gravity waves in the centimeter to decimeter wavelength region (Bragg waves pertaining to L, C, and X band radar backscattering) is probably more controlled by the hydrodynamic interaction with the long ocean surface waves [*Alpers et al.*, 1981] than by wave-induced air flow variations.

Assuming an infinite relaxation time [*Alpers et al.*, 1981], the maximum of the energy of the short waves appears at the crest of the long ocean wave. In contrast to L, C, and X band, a very strong frequency dependence of the phase of the MTF was measured at K_a band in the frequency range between 0.1 Hz and 0.35 Hz. Probably, this effect is caused by the wave-induced wind fluctuations. We expect that the modulation of the air flow near the sea surface is mainly determined by the dominant ocean wave. Therefore a stable phase for the generation of capillary waves exists only for this dominant wave, which has a low frequency. We suspect that for those waves which have smaller wavelengths than the dominant wave, the generation of short waves is more evenly distributed over the long wave profile.

APPENDIX

The Doppler shift f_d induced by the motion of the scatter element (facet) is given by

$$f_d = \pi^{-1} \vec{K} \cdot \vec{U} \tag{A1}$$

Here $\vec{K} = (K, K_3)$ denotes the three dimensional radar wave vector, K denotes its projection onto the horizontal plane, K_3 denotes its vertical component, and $\vec{U}$ the velocity of the facet.

The orbital velocity associated with ocean surface waves is given by [*Phillips*, 1977, p. 44]

$$U = \int \left(\omega \frac{k}{|k|} \frac{z(k)}{\tanh (kD)} e^{i(kx - \omega t)} + \text{c.c.} \right) dk \tag{A2}$$

$$U_3 = \int \left(e^{i\pi/2} \omega z(k) e^{i(kx - \omega t)} - \text{c.c.} \right) dk \tag{A3}$$

where D denotes the water depth, k the two-dimensional wave vector and ω the angular frequency of long ocean waves. Inserting (A2) and (A3) into equation (A1) yields

$$f_d = \frac{1}{\pi} \int \left[\left(\frac{k}{|k|} \cdot \frac{K}{\tanh (|k| \cdot D)} - iK_3 \right) \right.$$
$$\left. \cdot \omega z(k) e^{i(kx - \omega t)} + \text{c.c.} \right] dk \tag{A4}$$

Now we define the transfer function

$$S(k) = |S(k)| e^{i\phi_s(k)} \tag{A5}$$

which relates the Doppler shift f_d to the wave height ζ by

$$f_d = \int [S(k) z(k) e^{i(kx - \omega t)} + \text{c.c.}] dk \tag{A6}$$

We obtain from (A4)–(A6)

$$|S(k)| = \pi^{-1} \omega |\vec{K}| \left[\frac{\sin^2 \theta_i \cos^2 \phi}{[\tanh (|k| \cdot D)]^2} + \cos^2 \theta \right]^{1/2} \tag{A7}$$

$$\phi_s(k) = -\tan^{-1} \left[\frac{\cos \theta_i \tanh (|k| \cdot D)}{\sin \theta_i \cos \phi} \right] \tag{A8}$$

The last equation follows from

$$\tan \phi_s = \frac{\text{Im } S(k)}{\text{Re } S(k)} = -\frac{K_3 |k| [\tanh (|k| \cdot D)]}{k \cdot K} \tag{A9}$$

A negative ϕ_s means that the maximum of f_d occurs earlier than the maximum of ζ. Or expressed differently: If ϕ_s is negative, then the phase of f_d precedes the phase of ζ. In case of $\phi = 0°$ and infinite water depth $(D \to \infty)$ we obtain

$$\phi_s = -\theta_i \tag{A10}$$

The relationship between the power spectrum of the Doppler shift G_{f_d} and the power spectrum of the wave height associated with the long surface waves G_ζ reads

$$G_{f_d} = |S(k)|^2 \cdot G_\zeta \tag{A11}$$

where $|S(k)|$ is given by (A7).

REFERENCES

Alpers, W., and W. L. Jones, The modulation of the radar backscattering cross-section by long ocean waves, in *Proceedings of the 12th International Symposium on Remote Sensing of Environment*, pp. 1597–1606, Environmental Research Institute of Michigan, Ann Arbor, 1978.

Alpers, W., D. B. Ross, and C. L. Rufenach, On the detectability of ocean surface waves by real and synthetic aperture radar, *J. Geophys. Res., 86*, 6481–6498, 1981.

Bendat, J. S., and A. G. Piersol, *Measurement and Analysis of Random Data*, John Wiley, New York, 1966.

Elachi, C., Radar imaging of the ocean surface, *Boundary Layer Meteorol., 13*, 165–179, 1978.

Feindt, F. Radarrueckstreuexperimente am Wind-Wellen-Kanal bei sauberer und filmbedeckter Wasseroberflaeche im X-Band (9.8 GHz), Ph.D. thesis, Univ. of Hamburg, Federal Republic of Germany, 1985.

Keller, W. C., and J. W. Wright, Microwave scattering and the straining of wind-generated waves, *Radio Sci., 10*, 139–147, 1975.

Keller, W. C., and W. J. Plant and D. E. Weissmann, The dependence of X-band microwave sea return on atmospheric stability and sea state, *J. Geophys. Res., 90*, 1019–1029, 1985.

*Kitaigorodskii, S. A., *The Physics of Air-Sea Interaction* (in Russian), Gidrometeorologicheskoe Izdatel'stvo, Leningrad, 1970. (English translation, Israel Program for Scientific Translation, Jerusalem, 1973).

Phillips, O. M., *The Dynamics of the Upper Ocean*, 2nd ed., Cambridge University Press, New York, 1977.

Plant, W. J., W. C. Keller, and J. W. Wright, Modulation of coherent microwave backscatter by shoaling waves, *J. Geophys. Res., 83*, 1347–1352, 1978.

Plant, W. J., W. C. Keller, and A. Cross, Parametric dependence of the ocean wave–radar modulation transfer function, *J. Geophys. Res., 88*, 9747–9756, 1983.

Schröter, J., F. Feindt, W. Alpers, and W. C. Keller, Measurement of the ocean wave-radar modulation transfer function at 4.3 GHz, *J. Geophys. Res., 91*, 923–932, 1986.

Shemdin, O. H., W. E. Brown, Jr., F. G. Staudhammer, R. A. Shuchman, R. Rawson, J. Zelenka, D. B. Ross, W. McLeish, and R. A. Berles, Comparisons of in-situ and remotely sensed ocean waves off Marineland, Florida, *Boundary Layer Meteorol., 13*, 225–234, 1978.

Shuchman, R. A., W. Rosenthal, J. D. Lyden, D. R. Lyzenga, E. S. Kasischke, H. Guenther, and H. Linne, Analysis of MARSEN X-band SAR ocean wave data, *J. Geophys. Res.*, *88*, 9757–9768, 1983.

Wright, J. W., W. J. Plant, W. C. Keller, and W. L. Jones, Ocean wave-radar modulation transfer functions from the West Coast Experiment, *J. Geophys. Res.*, *85*, 4957–4966, 1980.

W. Alpers, Fachbereich 1 (Physik), Physik des Meeres, Universität Bremen, 2000 Bremen 33, Federal Republic of Germany.

F. Feindt, Institut für Meereskunde, Universität Hamburg, 2000 Hamburg 13, Federal Republic of Germany.

J. Schroeter, Max-Planck-Institut für Meteorologie, 2000 Hamburg 13, Federal Republic of Germany.